

Dark Matter Profiles in Clusters of Galaxies: a Phenomenological Approach

Yinon Arieli

School of Physics and Astronomy, Tel Aviv University, Tel Aviv, 69978, Israel

Yoel Rephaeli

*School of Physics and Astronomy, Tel Aviv University, Tel Aviv, 69978, Israel,
Center for Astrophysics and Space Sciences, University of California, San Diego,
La Jolla, CA 92093-0424*

Accepted for publication in New Astronomy

Abstract

There are some basic differences between the observed properties of galaxies and clusters and the predictions from current hydrodynamical simulations. These are particularly pronounced in the central regions of galaxies and clusters. The popular NFW (Navarro, Frenk, & White) profile, for example, predicts a density cusp at the center, a behavior that (unsurprisingly) has not been observed. While it is not fully clear what are the reasons for this discrepancy, it perhaps reflects (at least partly) insufficient spatial resolution of the simulations. In this paper we explore a purely phenomenological approach to determine dark matter density profiles that are more consistent with observational results. Specifically, we deduce the gas density distribution from measured X-ray brightness profiles, and substitute it in the hydrostatic equilibrium equation in order to derive the form of dark matter profiles. Given some basic theoretical requirements from a dark matter profile, we then consider a number of simple profiles that have the desired asymptotic form. We conclude that a dark matter profile of the form $\rho = \rho_0 (1 + r/r_a)^{-3}$ is most consistent with current observational results.

Key words: dark matter profiles - Galaxies: clusters: general - X-rays: galaxies: clusters

PACS: 98.65.Cw ; 95.35.+d ; 95.85Nv

¹ E-mail: yinonar@post.tau.ac.il

² E-mail: yoelr@noga.tau.ac.il

1 Introduction

Mass density profiles of galaxies and clusters of galaxies play a central role in the study of the intrinsic properties of these systems as well as in models of their formation, evolution, and their use as probes of the mass density of the universe. The formation of cold dark matter (CDM) halos has been studied extensively over the years. Considerable theoretical work has been done to describe the shape of DM profiles, mostly by numerical simulations (*e.g.*, Suto 2002). Early attempts were severely limited in predicting the profile in the central region due to insufficient spatial resolution. Recent improvements in numerical techniques led to the attainment of high central resolution (~ 10 kpc) in the dynamical simulation of DM profiles. However, a realistic description of the distribution of DM and gas in the central cluster regions necessitates a coupled dynamical and hydrodynamical simulation that can follow the evolution of DM and gas under their mutual interactions. In particular, heating and cooling processes in the gas can occur on timescales which are shorter than the Hubble time with possible ramifications also for the DM profile.

Based on large, N-body simulations of the evolution of DM configurations, Navarro, Frenk & White (hereafter NFW, 1995, 1997) showed that CDM density profiles are independent of the halo mass, and can be accurately fit over a large range of sizes by a simple algebraic form which is said to be universal (but see Jing & Suto 2000). The proposed NFW profile has a cusp-like r^{-1} behavior close to the center, and an asymptotic r^{-3} falloff at large r . It has been argued that DM profiles may even exhibit a steeper inner cusp; for example, Moore et al. (1999) claimed that high resolution simulations indicate that the central profile is $\propto r^{-1.5}$.

An uninterrupted steep rise of the density towards the center is clearly unphysical, and such a characterization could be due to insufficient level of spatial resolution in the numerical simulations, other important factors in the simulations (such as the particular choice of initial conditions, *e.g.*, Bartschiger & Labini 2001), or a result of physical limitations in the description of the cluster density over small ($O[10$ kpc]), typically *galactic* scales. That the latter are perhaps the more likely reasons is indicated by even a steeper inner cusp that is deduced in recent (Governato et al. 2001) higher resolution simulations. Even the improved hydrodynamical simulations do not include all the relevant physical processes that could affect the nature of the deduced mass profiles. For example, it is clear that the properties of intracluster (IC) gas, whose fractional contribution to the total mass is $\sim 10\%$, must play some role in the determination of the density profile.

Recent *Chandra* observations of the central regions of a few nearby clusters

have not (yet) provided unequivocal evidence on the shape of the central DM profile. Strong evidence was found for a flat profile in the central region of Abell 1795 (Ettori et al. 2002), a behavior similar to the trend seen in observations in some galaxies (mainly low surface brightness and dwarf galaxies). But there is also evidence for a central cusp in the clusters Abell 2029 (Lewis et al 2002), Hydra A (David et al. 2001), and EMSS 1358 (Arabadjis et al. 2002). However, evidence for the latter is weak, given the low quality of the fits (generally large χ^2/dof), central CD galaxy (in Abell 2029), low central resolution (in EMSS 1358), and relatively high value of the concentration parameter with respect to expectations from numerical simulations (in Hydra A). Clearly, many more *Chandra* and XMM observations of the central regions of clusters are needed in order to discern a clear trend in the shape of DM profiles there.

Over the last few years the NFW profile has been adopted in calculations of the structure and evolution of CDM halos, this in spite of its unappealing central cusp. There is a clear need for further exploration of cluster mass profiles with the aim of either modifying the NFW profile, or finding an alternative profile that is more consistent with observations. The inconsistency between observational results and predictions from simulations provides considerable motivation for a more *phenomenological* approach that is based on dynamical deductions from the observed properties of IC gas, an approach that is adopted in this paper. The gas density and temperature profiles can be determined from current high quality X-ray measurements; these profiles can then be used to probe the total density distribution.

We begin with a short review of IC gas density profiles, and their use to probe the DM profile based on the hydrostatic equilibrium (HE) equation. In section 3 we describe the limitations of the NFW profile for the IC DM density. Alternative DM profiles are discussed in section 4; we consider the requirements from a DM profile, and attempt a solution to the divergence problem of the NFW profile in section 4.1. This consists of a slight but physically important modification of the NFW profile which results in a finite density at the center. A theoretical discussion of new phenomenological DM profiles is given in section 4.2. Next (section 5), we confront several different DM profiles with observational data, primarily a sample of ROSAT measurements of 24 nearby and moderately distant clusters at redshifts $z \leq 0.2$, and draw some conclusions on the form of the most viable profile. In Section 6 we summarize and briefly discuss a few other aspects of the subject matter.

2 Spatial Distribution of IC Gas

Spectral measurements of thermal bremsstrahlung X-ray emission from IC gas provide an integrated measure of the emissivity-weighted temperature,

while the gas density profile is deduced from measurements of the surface brightness (SB) distribution across the cluster. A starting point in a theoretical description of the gas in a relaxed cluster is the attainment of HE, and although this includes aspherical configurations, the assumption of spherical symmetry is still reasonable for at least a subset of rich and regular clusters. The expected availability of uniform datasets of measurements of many clusters with the XMM and *Chandra* satellites motivates a more realistic modeling of the gas thermal and spatial distributions than afforded by an isothermal β model. An example for a more general description is a polytropic equation of state $P \propto \rho_g^\gamma$ relating the (thermal, assumed dominant) pressure and (*gas*) density, with the index γ as a free parameter. The HE equation is then

$$\frac{kT_0\gamma}{\mu m_p \rho_{g0}^{\gamma-1}} \rho_g^{\gamma-1} \frac{d \ln \rho_g}{dr} = -\frac{GM(r)}{r^2}, \quad (1)$$

where k , μ and m_p are the Boltzmann constant, the mean molecular weight, and the proton mass, respectively; $M(r)$ is the total cluster mass interior to r – a sum of the masses of DM, gas and galaxies.

The gas density is usually represented by an analytic (King) β profile

$$\rho_g(r) = \frac{\rho_{g0}}{[1 + y^2]^{3\beta/2}}, \quad (2)$$

with $y = r/r_c$; r_c is the gas core radius. In the case of isothermal gas, $\gamma = 1$, the (sky) projected X-ray SB profile that corresponds to this density is of the form

$$S_x^\beta(R) = S_0 \left(1 + \frac{R^2}{r_c^2}\right)^{-3\beta+1/2}, \quad (3)$$

where S_0 is the central SB, R denotes the projected distance from the cluster center, and β is a fit parameter. The X-ray deduced gas parameters are used in the HE equation to determine $M(r)$. In the simplest treatment the gas contribution to the gravitational field can be ignored, to first approximation, since the gas mass fraction is $\leq 10\%$.

3 The NFW Profile

The NFW DM profile is

$$\rho^{NFW}(x) = \frac{\rho_0}{x(1+x)^2}, \quad (4)$$

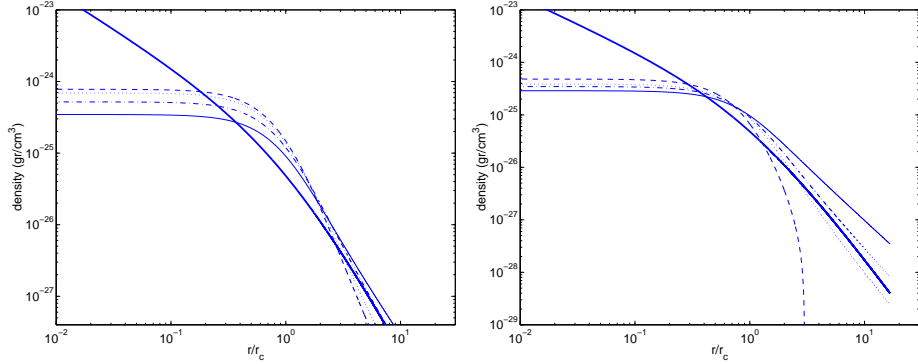


Fig. 1. DM density distribution obtained from the solution of the HE equation in the isothermal (left panel) and the more general polytropic (right panel) case are shown for various values of β and γ . Solid, dotted-dashed, dotted and dashed lines correspond to the results of the calculations for $\beta=2/3, 1, 4/3,$ and $3/2$ in the isothermal case, and $\gamma=1, 1.2, 4/3$ and $5/3$ in the polytropic case with $\beta = 2/3$, respectively. The thick solid line in each of the panels depicts the NFW profile.

where $x = r/r_s$; r_s is a scaling radial parameter. Both r_s and the central density ρ_0 are related to the cosmological parameters (NFW 1997). While it is generally deduced from N-body simulations that the DM density is asymptotically $\propto r^{-3}$, the behavior of the NFW profile in the inner core is problematic: There is no clear observational evidence for such density cusps in clusters. Specifically, the deduced mass distribution in clusters disagrees with that deduced from the NFW profile, and the X-ray SB calculated from this profile has a much smaller core radius than deduced from observations (Suto et al. 1998). Of course, the rise of density can be truncated below a certain inner radius and replaced by a constant value; this, however, is too arbitrary. The discrepancy is even larger in cD clusters.

3.1 DM profile from polytropic gas

We first show that there are appreciable differences between the DM profile deduced from an isothermal β gas and the NFW profile. The spherically symmetric HE equation – in the limit when the gas contribution to the gravitational field can be ignored – yields in this case

$$\rho^{poly}(y) = -\tilde{A} \frac{[(1+y^2)^{-3\beta/2}]^{\gamma-1} \{[-3\beta(\gamma-1)+1]y^2+3\}}{(1+y^2)^2}, \quad (5)$$

where $y = r/r_c$ and

$$\tilde{A} = \frac{3k\beta T_0}{4\pi G\mu m_p r_c^2}. \quad (6)$$

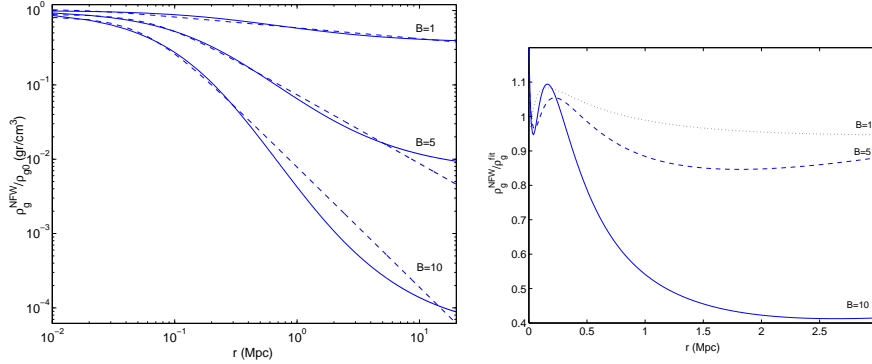


Fig. 2. The gas profiles deduced from substituting the NFW profile into the HE equation for different values of B ($B=1, 5$ and 10) are plotted as solid lines in the left panel. A dashed line next to each solid line shows the best fit to a β profile. The ratio between each profile and its best (β) fit is shown in the right panel.

In Figure 1 we show the resulting DM profiles and the NFW profile for typical values of the parameters; the left panel is for isothermal gas, while the right panel shows the results for $\gamma = 1.2, 4/3$ and $5/3$. There is a noticeable difference between these profiles and the NFW profile, especially at $r \leq r_c$. The calculated profiles converge to a constant central density, while the NFW profile diverges in this region. In the outer region the falloff of the NFW profile is more moderate than those of the other profiles.

Next we calculate the gas profile deduced from the NFW model; substituting the NFW profile (4) into the isothermal HE equation we have (as was obtained already by Suto, Sasaki & Makino 1998)

$$\rho_g(r) = \rho_{g0} \exp[-Bf(r/r_s)], \quad (7)$$

where

$$f(x) = 1 - \frac{1}{x} \ln(1+x), \quad (8)$$

for the NFW profile, and B is the dimensionless parameter

$$B \equiv \frac{4\pi G \mu m_p \rho_0 r_s^2}{kT_{g0}}. \quad (9)$$

In Figure 2 we plot the gas profiles deduced from the NFW profile for three values of B that correspond to a wide temperature range. Also shown are best fits of each of the three curves to a β profile. The right panel shows the ratio between each profile and its best-fit β profile. As can be seen in these figures the gas distribution deduced from the NFW profile is quite different from the

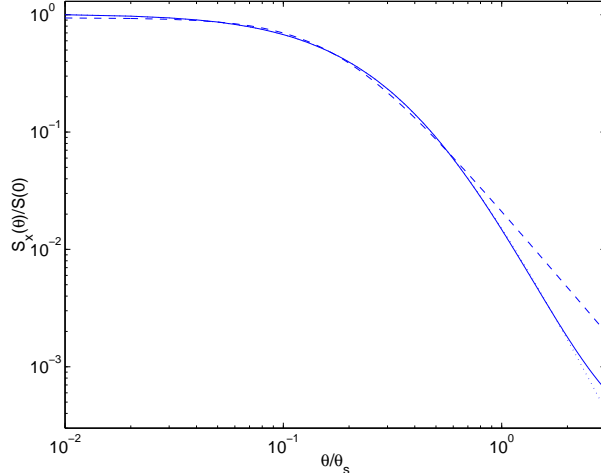


Fig. 3. The theoretical SB profile expected from substituting the NFW profile in the HE equation is plotted as solid line. The dashed and dotted lines are the best fit to a β surface brightness profile and a general β profile, respectively.

β profile. Only in the extreme and highly unlikely case of small B ($B \approx 1$) the two profiles are similar, with differences smaller than 10%.

Differences between the gas distribution deduced from the NFW profile and the β profile can also be demonstrated by their related X-ray SB. Fitting this predicted SB profile to the observed profile, which is known to have a β model shape, results in the dependence displayed in Figure 3.

Clearly, the SB predicted from the NFW profile does not provide a reasonably good fit to the β -model SB function. Rather, we find that the former function can be well fit by a generalized β distribution of the form

$$S_x^{new}(\theta/\theta_c) = \frac{S_x^{new}(0)}{\left[1 + (\theta/\theta_c^{new})^\xi\right]^{\tilde{\beta}}}, \quad (10)$$

where $\xi \neq 2$, and $\tilde{\beta} \neq 3\beta - 1/2$, i.e. values different than those of the β model (see dotted line in Figure 3). These results are consistent with those of Suto et al. (1998). Thus, it is clear that the general SB function S_x^{new} gives a better fit to S_x^{NFW} than does S_x^β .

We conclude that the NFW profile seems to be inconsistent with X-ray observations of clusters. The main physical reason for the above differences is the excessively high DM concentration that is predicted by the NFW model in the central cluster region.

Table 1

Upper limit on γ from the requirement that the gas profile is positive at $r \leq r_{max}$.

γ_{max}	1.07	1.16	1.38	1.07	1.15	1.35	1.06	1.13	1.32
r_{max} (Mpc)	1.5	1.5	1.5	2	2	2	3	3	3
B	20	10	5	20	10	5	20	10	5

3.2 The NFW profile and polytropic gas

When the NFW profile is substituted in the more general polytropic HE equation (1), the resulting gas density is

$$\rho_g(r) = \rho_{g0} \left[1 - \frac{B(\gamma - 1)}{\gamma} f(r/r_s) \right]^{\frac{1}{\gamma-1}}. \quad (11)$$

This function assumes negative values beyond a critical radius and is therefore physically unacceptable at larger radii.

For a cluster with a maximal radius r_{max} , the requirement that the profile is non-negative constrains the value of the polytropic index to be

$$\gamma \leq \frac{Bf(x_{max})}{Bf(x_{max}) - 1}, \quad (12)$$

where we took $x = x_{max}$ since $f(x)$ is a monotonically increasing function for the NFW profile. In table 1 we list the upper limit on the polytropic index for various values of r_{max} and B , with a typical value of the scale radius, $r_s = 0.2 \text{ Mpc}$. The results weakly depend on the value of the scale radius; for larger values of r_s , *e.g.*, 0.5 Mpc , the value of γ_{max} increases only by $\sim 5\%$. It would seem from Table 1 that in this model the polytropic index is limited to a relatively narrow range of values.

4 Alternative DM Profiles

Having discussed the possibly problematic features of the NFW model, we now want to find alternative DM profiles that are more physically viable and are consistent with X-ray SB measurements. To do so we first specify the properties desired of a DM profile, and then consider a slightly modified NFW profile, and – more generally – the simplest functional forms that satisfy the requirements from a DM profile. We require that a DM profile has the following properties:

1. Finite, positive-definite at all r .
2. Asymptotic r^{-3} behavior at large r .
3. An associated gas profile (from HE equation) that has the form of a β -profile with a value of β which is consistent with X-ray SB measurements.

The first property is an obvious physical requirement; the second is based on results of many N-body simulations, and the third is based on fits to observed SB profiles of many clusters. In assessing the viability of a DM profile we will also consider whether the central mass density is high enough for observable effects of gravitational lensing. In some clusters the measurements of either giant arcs, strong, or weak gravitational lensing imply that the DM central density needs to be sufficiently high to produce these lensing effects. Specifically, the central surface density has to be typically higher than the critical value of $\Sigma_0 \sim 0.5 \text{ gr/cm}^2$ (with $H_0 = 50 \text{ km s}^{-1} \text{ Mpc}^{-1}$ and $\Omega = 1$) in order that multiple lensed images are produced (Subramanian & Cowling 1986).

4.1 A Modified NFW profile

An operational approach to the divergence problem of the NFW profile is to replace it in the inner region, $r \leq r_b$, with a non-divergent form. From figures 1 & 2, it is clear that in the central region of the cluster the NFW profile is much steeper than either ρ^{iso} or ρ^{poly} , intersecting these curves inside the cluster core. Therefore, in order to remove the divergence of the NFW profile, in this inner region we replace the NFW profile with the functional form obtained as a solution – eq. (5) – to the HE equation when taking a β -profile for the gas. This form can then be tailored to the NFW profile outside the inner region, namely

$$\rho^{new-poly}(r) = \begin{cases} \tilde{A} \frac{\left\{ [1+(r/r_c)^2]^{-3\beta/2} \right\}^{\gamma-1} \left\{ [-3\beta(\gamma-1)+1](r/r_c)^2+3 \right\}}{[1+(r/r_c)^2]^2} & r \leq r_b \\ \frac{\rho_0}{(r/r_s)(1+r/r_s)^2} & r > r_b \end{cases}, \quad (13)$$

for the (general) polytropic case.

The new modified profile is not smooth at $r = r_b$, but it is continuous at this point, and at larger radii it falls off asymptotically as r^{-3} . If we were to fit it by the functions of the kind of ρ^{iso} and ρ^{poly} , the fit would be excellent in the central region, but the quality of the fit would deteriorate outside this region. Thus, the overall discrepancy between this modified DM profile and the profile

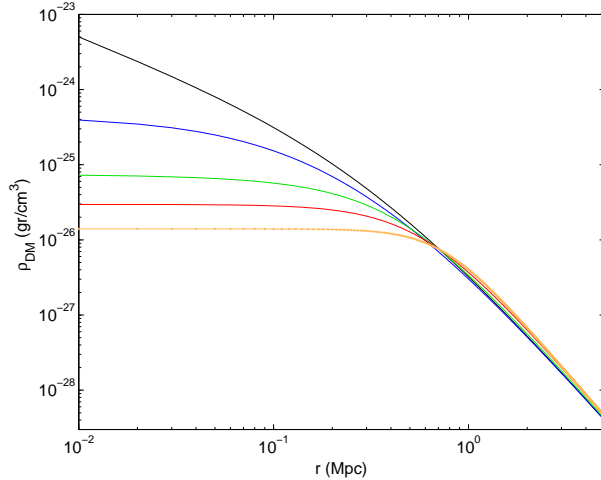


Fig. 4. The DM profiles $\rho^I - \rho^{IV}$ are plotted in blue, green, red and orange lines, respectively; the black line shows the NFW profile.

deduced from the measured gas density would still remain. (Note that the DM profile can be similarly changed in clusters with a giant cD galaxy whose DM density distribution is generally different from the NFW profile.)

4.2 New DM profiles

Adopting a purely phenomenological approach we can readily write down a family of DM profiles that satisfy the first two requisite properties, resembling an isothermal profile in the inner region and falloff asymptotically as r^{-3} at large radii. These profiles can be characterized by a scale radius r_a (which is generally different from the NFW scale radius r_s), and the set of three parameters (η, ν, λ) :

$$\rho = \frac{\rho_0^*}{[1 + x^\eta][1 + x^\nu]^\lambda}, \quad (14)$$

for which $\eta + \nu + \lambda = 3$, and $x = r/r_a$. Here we consider the four simplest profiles characterized by $(\eta, \nu, \lambda) = (0, 1, 3)$, $(1, 2, 1)$, $(0, 2, 3/2)$ and $(3, \nu, 0)$, with $\rho_0^* = 2\rho_0$ for $\eta = 0$, and $\rho_0^* = \rho_0$ for $\eta = 1, 3$. The second profile was previously deduced to provide a good fit to the distribution of DM in dwarf galaxies (Berkert, 1995).

In order to be able to meaningfully compare the different models, we take a nominal value of $10^{15} M_\odot$ for the total mass of the cluster (mostly that of the DM and gas) at the virial radius, $r_{vir} \approx 1.5 Mpc$. Doing so relates the central density and scale radius, so the values of these quantities cannot be arbitrarily selected. The requirements of the equality of the total masses at the

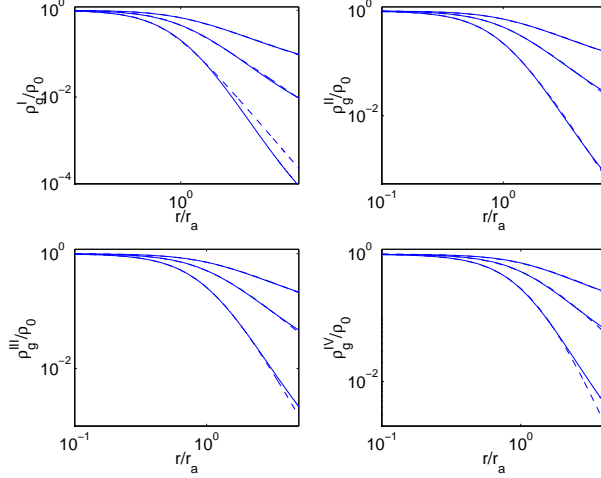


Fig. 5. Gas profiles obtained from substituting the new DM profiles into the HE equation (solid lines) and the best fit to a β -profile (dashed lines). Results for the first and second profiles are shown in the upper right and left panels, and those for the third and fourth profiles are in lower right and left panels, respectively. In each panel the upper to lower graph are for the cases corresponding to $B = 5, 10,$ and $20,$ respectively.

virial radius and the r^{-3} falloff at large radius completely specify the profile parameters. The four new DM profiles are shown in figure 4 together with the NFW profile. Clearly, values of the central densities span a wide range, and the convergence of the first profile (ρ^I) to the asymptotic r^{-3} law is the fastest.

To check whether the third condition is also satisfied, we substitute the new profiles into the HE isothermal equation, neglecting the gas and galaxy contributions to the total mass, and obtain the following gas profiles,

$$\rho_g^i(x) = \rho_{g0}^i \exp[-Bf^i(x)] \quad (15)$$

where

$$f^I(x) = \frac{2+x}{2+2x} - \frac{\ln(1+x)}{x} \quad (16)$$

$$f^{II}(x) = \frac{1}{4x} \left\{ 2(1+x) [\arctan(x) - \ln(1+x)] + (x-1) \ln(1+x^2) \right\} \quad (17)$$

$$f^{III}(x) = 1 - \frac{\text{arcsinh}(x)}{x} \quad (18)$$

$$f^{IV}(x) = \frac{1}{6x} \left[3x^3 {}_2F_1 \left(\frac{2}{3}, 1, \frac{5}{3}, -x^3 \right) - 2 \ln(1+x^3) \right] \quad (19)$$

where ${}_2F_1$ is the hypergeometric function. The parameter B was, defined in eq. (9), depends on the DM parameters r_a and ρ_0 , and the gas parameters T_0

Table 2

Values of B characterizing the DM profile for central temperatures in the range of 5-15 keV.

B_{NFW}	B_I	B_{II}	B_{III}	B_{IV}
20	35.13	18.94	13.64	11.39
10	17.56	9.47	6.82	5.69
5	8.78	4.73	3.41	2.84

and β . Due to the stipulated constancy of the mass at the virial radius, B essentially depends only on the gas temperature, T_0 . In Table 2 we list values of B for temperatures in the range 5-15 keV.

Fits of the new gas profiles to a β model are shown in figure 5. Although all the fits provide better approximation to the β model than the corresponding fit from the NFW model, values of the fit parameters for the third and fourth profiles are somewhat unlikely. The second profile yields good results only on small scales ($r \leq 0.7 - 0.8 Mpc$); the fit is poor at larger radii. The best fit is obtained with the first profile.

We checked whether each of the above DM profiles can be closely approximated by fitting a solution of the HE equation obtained with an isothermal β profile for the gas. The fit parameters were $\tilde{A}, r_c, \rho_{g0}$ and β . Not surprisingly, we find that all of the above four profiles can be very well fit by a solution of the HE equation. Here again the fit to the NFW profile is very poor. We have also compared the gas profiles deduced from the HE equation for each of the DM models directly to the observed quantity by numerically evaluating the SB. (In these computations the gas density was truncated at $x = 20$, corresponding to a limiting radius which is larger than the virial radius.)

Results of the fits of the deduced SB profiles to a β model are shown in Figure 6. The first two profiles yield good fits to a SB that has a form of a β profile, with reasonable parameter values. The third and fourth profiles are better fit by a function of the form of S_x^{new} (Eq. 10), with $\xi \neq 2$ and $\tilde{\beta} \neq 3\beta - 1/2$, as does the modified NFW model.

Next we derived the gas density distributions from the HE equation for polytropic gas and with the DM mass corresponding to the above profiles. The deduced gas density profiles are represented in terms of the function $f(r)$ in eq. (11). Since this function is monotonically increasing with r , there is an upper limit on the value of γ below which the density is positive definite. We have determined the limiting values of γ for typical values of B and $r_{max} = 1.5 Mpc$. Only for the first DM profile these limits are acceptable. For the other three profiles the deduced values of γ are either unrealistic or negative, and thus unacceptable for the observed range of gas temperatures.

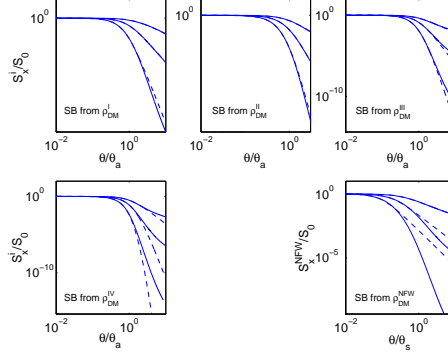


Fig. 6. The SB obtained from substituting each DM profile into S_x is shown by a solid line, and the best fit to a SB β -profile is plotted as a dashed line. The cases corresponding to $B = 10, 15$ and 20 are shown in each figure from the upper to the lower lines, respectively. Also plotted are the results for the SB corresponding to the NFW profile.

As discussed previously, the mass obtained from the HE equation for isothermal gas closely approximates the cluster total mass since the gas is approximately isothermal and the fractional mass contribution of the gas is small. We have compared the DM masses obtained from direct integrations of the DM density distributions and those obtained from the HE equation for isothermal gas. For isothermal gas, the deduced cluster mass is

$$M^{iso}(r) = \frac{3kT_0\beta}{\mu m_p Gr_c^2} \frac{r^3}{\left(1 + \frac{r^2}{r_c^2}\right)}. \quad (20)$$

The DM mass profiles for the new profiles can be written as

$$M(r) = 4\pi\rho_0 r_a^3 m(x), \quad (21)$$

where $m(x)$ are obtained by integrating the four profiles:

$$m^I(x) = \ln(1+x) - \frac{x(2+3x)}{2(1+x)^2} \quad (22)$$

$$m^{II}(x) = \frac{1}{4} \left[2\ln(1+x) + \ln(1+x^2) - 2\arctan(x) \right] \quad (23)$$

$$m^{III}(x) = \operatorname{arcsinh}(x) - \frac{x}{\sqrt{1+x^2}} \quad (24)$$

$$m^{IV}(x) = \frac{1}{3} \ln(1+x^3). \quad (25)$$

The new profiles can be well described by such a function, while only a poor fit is obtained to the NFW mass profile.

Finally, the presence of gravitational arcs in some clusters implies sufficiently high central mass densities. We have evaluated the central surface densities for the new profiles using the Abel integral; these are

$$\Sigma^I(0) = \rho_0^I r_a^I \quad (26)$$

$$\Sigma^{II}(0) = \frac{\pi}{2} \rho_0^{II} r_a^{II} \quad (27)$$

$$\Sigma^{III}(0) = 2\rho_0^{III} r_a^{III} \quad (28)$$

$$\Sigma^{IV}(0) = \frac{4\pi}{3\sqrt{3}} \rho_0^{IV} r_a^{IV} \quad (29)$$

for the first to the fourth profile. Actual values are ~ 1 g/cm² for the first DM profile, to about a factor ~ 4 lower for the fourth profile. Since these values are quite comparable to the critical density $\Sigma_c \approx 0.5$ g/cm² needed to produce arcs, no additional constraint is imposed on these models by this consideration.

5 Parameters of the DM profiles from a ROSAT Sample

In an attempt to further distinguish between the four DM profiles described in the previous section and possibly select the most realistic profile based on available observational data, we have used results from a sample of SB profiles of clusters measured with the ROSAT PSPC. The sample – a subset of a dataset which was compiled and investigated by Ettori & Fabian (1999; the data were kindly provided by Ettori) – consists of 24 clusters with X-ray luminosities $\geq 10^{45}$ erg s⁻¹ (taking $H_0 = 50$ km s⁻¹ Mpc⁻¹), at redshifts in the range 0.051 – 0.203. We have selected nearby and moderately distant clusters for which the ROSAT PSPC provides some – albeit not optimal – spatial resolution (for more details, see Ettori & Fabian 1999). We performed fits of the measured SB profiles to those predicted from three different models for the isothermal gas density. The assumption of gas isothermality is a reasonable approximation to the temperature profile at radii larger than $0.1r_{vir}$ (≈ 0.2 Mpc). All three models were deduced from the HE equation adopting these DM profiles: NFW, and our first (ρ^I) and second (ρ^{II}) models. The corresponding gas density distributions are

$$\rho_g^N(x) = \rho_{g0}^N \exp^{-B_N} (1+x)^{B_N/x}, \quad (30)$$

where $x = r/r_s$,

$$\rho_g^I(x) = \rho_{g0}^I \exp^{-\frac{B_I(2+x)}{2+2x}} (1+x)^{B_I/x}, \quad (31)$$

Table 3

Parameters of DM profiles from fits to the SB data, and reduced χ^2 of the fits. σ_χ is the standard deviation for the reduced χ^2 , and the scale radius is in Mpc.

cluster	z	Fitting Parameters			Goodness of the fit			
		r_a, B_I	r_a, B_{II}	r_s, B_N	χ_I^2	χ_{II}^2	χ_N^2	σ_χ
A401	0.0748	0.29 , 14.88	0.32 , 8.51	0.87 , 8.92	1.69	2.33	1.92	0.20
A478	0.0881	0.17 , 16.28	0.19 , 9.35	0.50 , 9.61	5.71	18.75	2.98	0.35
A520	0.203	0.59 , 19.31	0.56 , 10.08	2.73 , 15.01	1.19	1.03	1.70	0.33
A545	0.153	0.45 , 19.31	0.44 , 10.39	1.66 , 13.1	1.49	0.97	2.89	0.45
A586	0.171	0.22 , 16.43	0.24 , 9.27	0.68 , 9.88	1.38	1.10	1.98	0.33
A644	0.0704	0.24 , 16.07	0.25 , 9.10	0.68 , 9.50	2.87	2.45	4.30	0.28
A1413	0.1427	0.22 , 16.24	0.24 , 9.21	0.69 , 9.86	1.97	2.94	2.10	0.32
A1651	0.0825	0.24 , 15.67	0.25 , 8.82	0.63 , 8.96	1.82	1.68	1.72	0.28
A1656	0.0232	0.54 , 18.76	0.54 , 10.29	2.20 , 13.09	1.16	0.98	3.39	0.32
A1689	0.181	0.22 , 17.55	0.24 , 9.94	0.70 , 10.71	2.69	5.40	2.08	0.3
A1763	0.187	0.36 , 15.79	0.38 , 8.90	1.15 , 9.76	4.03	6.32	2.36	0.39
A2029	0.0765	0.14 , 15.06	0.16 , 8.71	0.40 , 8.80	3.55	11.15	4.19	0.39
A2163	0.203	0.41 , 15.86	0.42 , 8.75	1.40 , 10.21	1.37	1.35	2.52	0.34
A2204	0.1523	0.15 , 15.96	0.17 , 9.22	0.43 , 9.29	0.83	1.29	0.93	0.38
A2218	0.175	0.34 , 17.21	0.35 , 9.49	1.19 , 11.17	1.00	1.30	2.76	0.31
A2244	0.097	0.18 , 15.68	0.20 , 9.04	0.54 , 9.30	1.06	1.23	1.44	0.24
A2255	0.0809	0.86 , 21.53	0.76 , 10.62	6.91 , 26.09	0.99	1.14	0.95	0.21
A2319	0.0559	0.31 , 14.12	0.36 , 8.15	0.94 , 8.49	3.02	5.21	1.46	0.22
A2507	0.196	0.58 , 16.04	0.56 , 8.52	2.97 , 13.39	1.02	0.95	1.08	0.21
A3112	0.0746	0.11 , 15.23	0.15 , 9.02	0.29 , 8.85	1.44	2.15	1.61	0.27
A3667	0.0542	0.32 , 13.29	0.34 , 7.49	1.02 , 8.22	4.99	7.81	5.33	0.35
A3888	0.168	0.47 , 22.09	0.47 , 12.24	2.38 , 18.15	1.54	1.65	1.60	0.16
PKS0745	0.1028	0.13 , 16.19	0.15 , 9.42	0.38 , 9.52	2.85	3.47	4.65	0.25
Triang	0.051	0.38 , 15.87	0.41 , 8.91	1.85 , 9.84	3.86	6.29	2.06	0.23

and

$$\rho_g^{II}(x) = \rho_{g0}^{II} \exp^{-\frac{B_{II}}{4x} \{2(1+x)[\arctan(x) - \ln(1+x)] + (x-1) \ln(1+x^2)\}}, \quad (32)$$

where $x = r/r_a$. The fits were performed by χ^2 minimization (using the 'Minuit' CERN program).

Results of the fits are summarized in Table 3, where in addition to listing the best-fit values of the scale radii and B , values of the reduced χ^2 (χ^2/dof) and the standard deviation for the reduced χ^2 are also specified. Of the three models, the first DM profile provides the best fit to the data of 11 out of the 24 clusters, with the second profile providing the best fit in 8 clusters. Furthermore, for most of the latter 8 clusters the differences between the quality of the fits based on the first and second DM models are not statistically significant. Based on the results from this ROSAT dataset it is apparent that the first DM profile is most consistent with the data while the NFW profile is the least favored. (We note that all three fits to the data on three clusters – A478, A1763 & A3667 – are very poor, raising doubts on the validity of the assumption of hydrostatic equilibrium of the gas in these clusters, perhaps due to ongoing merger activity?).

In order to assess the impact of a more precise but similar database, we have repeated the fits by artificially reducing the observational errors in the measurements of the SB. Doing so does not affect appreciably the quality of the fit to the SB from the first DM model, but reduces the consistency with the second DM model and significantly worsening the viability of the NFW profile. Clearly, since this test is based on the current database it does not add independent confirmation of the results, but rather just a simulation of what might be feasible to do when higher quality data become available.

6 Discussion

The aim of this work has been to find alternative DM profiles that are finite at the cluster center and are consistent with observed X-ray SB profiles. Our approach is purely phenomenological and is based on the selection of simple non-cusped profiles that falloff asymptotically as $\propto r^{-3}$ at large r . We first constructed two modified NFW profiles (ρ^{iso} and ρ^{poly}) by truncating the NFW below some inner radius (r_b) merely to remedy the central divergence of the NFW model. Since $r_b \sim 50$ kpc, the new profiles quickly converge to the NFW profile. But the requirement that the related gas density profile has an associated thermal bremsstrahlung SB with the typical β model shape led us to abandon these modified profiles as realistic alternatives to the NFW model.

We then considered four new profiles characterized by the three parameters (μ, ν, λ) with the requisite features, and tested their viability by contrasting their associated SB profiles with ROSAT data on a sample of 24 clusters. Comparison of the gas profiles resulting from the new DM models with β gas

profiles clearly shows that all of these give better results than the NFW profile. Below a radius of about 1 Mpc, the behavior of all four profiles is acceptable, but progressively degrades at larger radii. Examining the SB profile calculated from the different DM profiles we saw that the results are not unequivocal, namely that the general shape of the SB function can be fitted quite well to a β SB profile. This is so for a fit done over a large range of radii; the fit is particularly good over the radial range $r \leq 1.5 - 2 \text{ Mpc}$. The reason for this is the fact that a SB that has the shape of a β profile necessarily has a flat slope in the central region. Upon detailed comparison of the results of the fits, as well as consistency with polytropic gas distributions, we concluded that the first of these four profiles, for which $(\eta, \nu, \lambda) = (0, 1, 3)$:

$$\rho(r) = \frac{\rho_0}{(1 + r/r_a)^3}, \quad (33)$$

is most consistent with the ROSAT sample. We emphasize, however, that due to the large observational uncertainties the preference of the first profile over the second is not large. It is quite likely that the availability of more precise X-ray SB and temperature measurements will enable a more definite distinction to be made between these viable alternatives to the NFW profile.

Independent recent work (El-Zant, Shlosman & Hoffman 2001) also leads to a resolution of the 'core catastrophe' in galaxies – the discrepancy between the diverging inner density profile of DM from CDM N-body simulations and the finite core deduced from observations. These authors suggest the gas in galaxies is not initially smoothly distributed in the DM halo, but rather is concentrated in small clumps containing $\sim 0.01\%$ of the total mass. The orbital energy of the clumps dissipates by dynamical friction as they move in background of DM particles, thereby transferring energy to the DM and heating it. This process is said to be sufficiently effective to turn the primordial cusp of the DM profile into a non-diverging core, resulting in a profile of the form

$$\rho = \frac{C}{(r + r_c)(A + r)^2}, \quad (34)$$

where C is a fixed parameter, A and r_c are a scale parameter and core radius, respectively. Furthermore, it was found that best fits require that $A = r_c$, which then yields essentially the same profile that we have deduced for clusters. This similarity between the behavior of the DM profile in galaxies and in clusters is indeed expected in theories of formation and evolution of the large scale structure. Gravitational drag could also be important in clusters (e.g., Rephaeli & Salpeter 1980), so a similar process of transfer of kinetic energy of the galaxies (initially with their DM halos) to the IC DM could have flattened also cluster profiles.

Flattening of DM profiles in the centers of galaxies and clusters is suggested by other theoretical considerations. For example, D’Onghia, Firmani & Chincarini (2002) have recently argued that the flattening can occur in galactic and cluster centers if the DM in these systems consists of weakly self-interacting particles. Collisions between the particles during system collapse and the associated inward transfer of heat lead to expansion of the core. They propose that this process is implemented in N-body simulations by modifying the initial conditions and taking a self-interaction cross section that is inversely proportional to the particle velocity.

Finally, the physical motivation to find a more acceptable form for DM density profiles in galaxies and clusters, and the already available observational data, provide a viable basis for selecting between simple, well-behaved profiles. We have identified what seems to be the most consistent form of the DM distribution in clusters. Our work has been based on a simplified theoretical description of clusters – such as the sphericity of the cluster and isothermality of IC gas – assumptions that can be relaxed when higher quality spectral and spatial XMM and *Chandra* measurements of clusters will be available.

ACKNOWLEDGEMENTS

We are grateful to Dr. Stefano Ettori for providing the ROSAT dataset discussed in this paper.

References

- Arabadjis J.S., Bautz M.W. & Garmire G.P., 2002, ApJ 572, 66-78.
- Baertschiger, T. & Labini F.S., astro-ph/0109199.
- Burkert, A., astro-ph/9504041.
- David, L.P. et al, 2001, ApJ 557, 546-559.
- D’Onghia, E., Firmani C. & Chincarini G., astro-ph/0203255.
- El-Zant, A., Shlosman I. & Hoffman Y., astro-ph/0103386.
- Ettori, S. & Fabian A.C., astro-ph/9901304.
- Ettori, S. & Fabian A.C., Allen S.W & Johnstone R.M., 2002, MNRS 331, 635-648.
- Governato F., Ghigna S. & Moore B., astro-ph/0105443.
- Jing, Y.P. & Suto Y., 2000, ApJ 529, L000.

Lewis, A.D., Boute D.A. & Stocke J.T., asrto-ph/0209205.
Moore, B., Quinn T., Governato F., Stadel J. & Lake G., astro-ph/9903164.
Navarro, J., Frenk C.S.& White S.D.M., 1995, MNRAS 275, 720.
Navarro, J., Frenk C.S.& White S.D.M., 1997, ApJ 490, 493.
Rephaeli, Y. & Salpeter E.E., 1980, ApJ, 240, 20.
Subramanian, K. & Cowling S.A., 1986, MNRS., 219,333-346.
Suto, Y. Sasaki, S. & Makino N., astro-ph/9807112.
Suto, Y. Sasaki, S. & Makino N., 1998A, ApJ 497,555.
Suto, Y., astro-ph/0207202.

